



Uniaxial stress identification of steel components based on one dimensional-CNN and ultrasonic method

Lu Deng^{a,b}, Shaopeng Xu^b, Wei Wang^{a,b,*}, Chao Xiang^b

^a Key Laboratory for Damage Diagnosis of Engineering Structures of Hunan Province, Hunan University, Changsha, Hunan 410082, China

^b College of Civil Engineering, Hunan University, Changsha, Hunan 410082, China

ARTICLE INFO

Keywords:
Stress identification
One-dimensional CNN
Steel component
Deep learning
Ultrasonic technique

ABSTRACT

The absolute stress of steel components is a key parameter in the construction and service of steel structures. Traditional stress testing methods have drawbacks of high cost and low accuracy. A new method based on deep learning and ultrasonic technique is proposed to obtain the absolute stress of steel components with different thicknesses. Firstly, ultrasonic signals of steel components under different stress levels were collected and used to build datasets. Secondly, the optimal architecture of one-dimensional convolutional neural networks (CNNs) for stress identification of steel components was determined. Finally, parameters of the network with the optimal architecture were optimized and used to identify the absolute stress of the unknown test dataset. The results show that the average stress identification error for the unknown test dataset is 3.83%. The proposed method can overcome the drawbacks of conventional techniques and provide good references for stress identification of steel components in practical engineering.

1. Introduction

In recent decades, steel structures have been widely used in modern construction due to its high strength, light weight, good seismic performance, and recyclability. Obtaining absolute stress in steel components is very important for assessing the safety, estimating the remaining life, and determining the reinforcement and renovation schedule of the steel structures [1]. Nondestructive testing methods have been widely used to detect the stress of steel structures, which will not cause damage to the structure. Nondestructive testing methods mainly include electrical detection (resistive strain gauge [2] and vibrating wire strain gauge [3]), X-ray diffraction [4], magnetic detection (Magnetic Barkhausen Noise [5] and metal magnetic memory testing [6]), and ultrasonic method [7]. However, the electrical detection method can only detect the stress increment of structures but not the absolute stress of the structure. The magnetic detection method can only be used for the identification of stress in ferromagnetic materials. The X-ray diffraction method requires expensive equipment and a severe detection environment. The ultrasonic method can measure the surface stress and internal stress of structures, and the required measuring instruments are portable and inexpensive. Therefore, the ultrasonic method has a broad prospect

in the field of nondestructive testing.

Actually, in 1953, Hughes and Kelly [8] proposed the acoustoelasticity theory for isotropic materials and established the relationship between the propagation speed of ultrasound waves and stresses in materials. In 1959, Benson and Raelson [9] proposed a new method to determine the uniaxial stress in isotropic materials using polarized transverse acoustic waves, and introduced the concept of "acoustoelastic effect". In 1973, Nelson N. Hsu [10] designed a new technique for stress identification based on ultrasonic waves. Based on the acoustoelasticity theory, the ultrasonic signal characteristics are different when the steel component is under different stress levels, which makes it possible to use ultrasonic waves to identify the absolute stress of steel components. Based on the characteristics of wave propagation, the ultrasonic waves can be divided into five categories, including the shear wave, longitudinal wave, surface wave, critical refracted longitudinal wave (L_{cr} wave), and guided wave. The utilization of longitudinal wave and L_{cr} wave for absolute stress detection usually needs to obtain the ultrasonic characteristic parameters of the zero-stress state in advance, which is sometimes difficult to achieve in actual situations. Surface wave cannot be utilized to accurately detect the internal stress in steel components due to its poor penetration ability. The guided wave can propagate a

* Corresponding author at: Key Laboratory for Damage Diagnosis of Engineering Structures of Hunan Province, Hunan University, Changsha, Hunan 410082, China.

E-mail addresses: dengl@hnu.edu.cn (L. Deng), xsp@hnu.edu.cn (S. Xu), wang_wei@hnu.edu.cn (W. Wang), xiangchao@hnu.edu.cn (C. Xiang).

long distance with little attenuation, but it has complex dispersion characteristics which make the stress detection operation difficult and often highly depend on senior technical engineers for data analysis. A shear wave is a waveform whose oscillations are vertical to the direction of the wave's propagation, and the acoustic anisotropy of the material is related to the shear-wave polarization direction. The ultrasonic shear wave will decompose into two separated wave components when perpendicularly emitting to the stress surface, and the shear-wave components parallel to the stress and perpendicular to the stress have different wave velocities, which is called the shear-wave birefringence effect [11]. It was found that the velocity difference between the two separated wave components of the shear wave is proportional to the magnitude of stress and can be used to measure the stress [12]. Therefore, the ultrasonic shear wave was selected for absolute stress identification of steel components based on the phenomenon of the ultrasonic shear-wave birefringence.

Based on the ultrasonic technique, some scholars conducted lots of studies on structure stress detection. In 2016, Li et al. [13] used the acoustic time-of-flight method (TOF) to identify the absolute axial stress of steel members and compared the results to those obtained from the strain gauge method. Later, he [14] derived the relationship between the axial absolute stress and the amplitude spectrum characteristics of steel components based on the ultrasonic shear-wave amplitude spectrum and found that the error between the calculated stress and the true stress was less than 5%. In 2018, He et al. [15] obtained the absolute stress distribution and stress extremes of steel components based on the critical refracted longitudinal wave (L_{cr} wave). Subsequently, he also compared the performance of the L_{cr} wave-based TOF method with the ultrasonic shear-wave amplitude spectrum method for the identification of steel stress and found that the amplitude spectrum method was less affected by high-frequency noise than the TOF method [16]. It should be noted that the stress identification methods proposed in the above study were applied only for steel components with a single thickness rather than those with different thicknesses, which may limit the application of the above methods.

With the rapid development of deep learning, plenty of scholars used the CNN to classify the response signals (acoustic emission signals, vibration signals, etc.) or images of structures, to better identify damages of structures. Zhang et al. [17] combined the CNN and acoustic emission to identify the damage of steel rails. Li et al. [18] used the synchronous compression wavelet transform and multi-branch CNN to classify the acoustic emission signals of steel rails, and adopted the Bayesian optimization algorithm to determine the network hyperparameters. Based on the vibration signals, Chen et al. [19] used the CNN to identify the damage of gearboxes, and Kim and Choi [20] combined the signal segmentation techniques and CNN to realize the diagnosis of gear faults. Based on the microscopic features of steel component surface, Wang et al. [21] realized the classification of six different absolute stresses of steel components with the Faster R-CNN, which provided a new perspective for the absolute stress identification of steel members. Wu et al. [22] used a one-dimensional CNN (1-D CNN) to classify the vibration signals of oil pipelines and compared it with a two-dimensional CNN to demonstrate the superiority of 1-D CNN. Zhang et al. [23] directly input the raw acceleration signal of a steel beam into a 1-D CNN to realize the classification of structure states. Eren et al. [24] achieved the classification of bearing faults based on the vibration signal of an electric motor through a 1-D CNN and found that the 1-D CNN could enhance the computational efficiency without reducing the accuracy. As mentioned above, the CNNs have been widely used for signal processing to realize structural damage detection, among which the 1-D CNN is especially good at classifying response signals of structures. However, few studies are focusing on stress identification of steel components based on the 1-D CNN and ultrasonic method.

In the present study, a low-cost, high-accuracy, and easy-to-operate method is proposed for absolute stress identification of steel components with different thicknesses based on the advantages of deep

Table 1
Three designed architectures of 1-D CNNs for stress identification.

Type of layer	Kernel information	Shadow	Medium	Deep
Conv1D_1	Kernel number Kernel size	16 64	16 64	16 64
Maxpooling1D_1	Kernel size	2	2	2
Conv1D_2	Kernel number Kernel size	32 3	32 3	32 3
Maxpooling1D_2	Kernel size	2	2	2
Conv1D_3	Kernel number Kernel size	64 3-	64 3	64 3
Maxpooling1D_3	Kernel size	2	2	2
Conv1D_4	Kernel number Kernel size	128 3	128 3	128 3
Maxpooling1D_4	Kernel size	2	2	2
Conv1D_5	Kernel number Kernel size	– 3	256	256 3
Maxpooling1D_5	Kernel size	– 2	2	2
Conv1D_6	Kernel number Kernel size	– 3	256	256 3
Maxpooling1D_6	Kernel size	– 2	2	2
Conv1D_7	Kernel number Kernel size	– 3	– 256	– 256
Maxpooling1D_7	Kernel size	– –	– 2	– 2
Conv1D_8	Kernel number Kernel size	– 3	– 256	– 3
Maxpooling1D_8	Kernel size	– –	– 2	– 2
GlobalAverage-Pooling1D	–	Yes	Yes	Yes
Fully Connected layer	Number of nodes	64	–	128
LinearRegression	Number of nodes	1	1	1
Number of parameters		41,841	329,201	755,697

learning and the ultrasonic technique. Firstly, the ultrasonic signals of steel components under different stress levels were collected in the laboratory through the uniaxial compression test to establish ultrasonic signal datasets. The training and validation datasets consist of ultrasonic signals obtained under ten stress levels ranging from 0 to 300 MPa, and the test dataset consists of ultrasonic signals obtained under nine different stress levels of 14, 30, 52, 74, 96, 142, 196, 260, and 306 MPa, respectively. Secondly, three 1-D CNN architectures were designed, trained and tested with the prepared datasets and the optimal architecture was determined for stress identification of steel components. Finally, the parameters of the network with the optimal architecture were optimized and then used to identify the absolute stress of the test dataset and the results show that the proposed method has good robustness in identifying the absolute stresses of steel components with different thicknesses.

The rest of the study is organized as follows. The design of the one-dimensional CNN network is described in Section 2. Section 3 describes the details on the laboratory experiment, dataset preparation, determination and optimization of the 1-D CNN model. In Section 4, the conclusions of the study are drawn and future directions for research are outlined.

2. One-dimensional CNN for stress identification

2.1. Architecture design of the one-dimensional CNN

The CNN is a representative algorithm of deep learning and is widely used in computer vision, natural language processing, and structural damage detection [25]. Compared to deep neural networks (DNNs), the sparse connectivity and weight sharing operations of the CNN can significantly reduce the number of parameters and thus accelerate the process of training. The pooling layer of CNN can also preserve features and prevent over-fitting [26]. The 1-D CNN inherits the advantages of CNN and excels in handling 1-D time series data. Three 1-D CNNs with different architectures, as shown in Table 1, were designed to process the ultrasonic signal collected in the study to determine the optimal

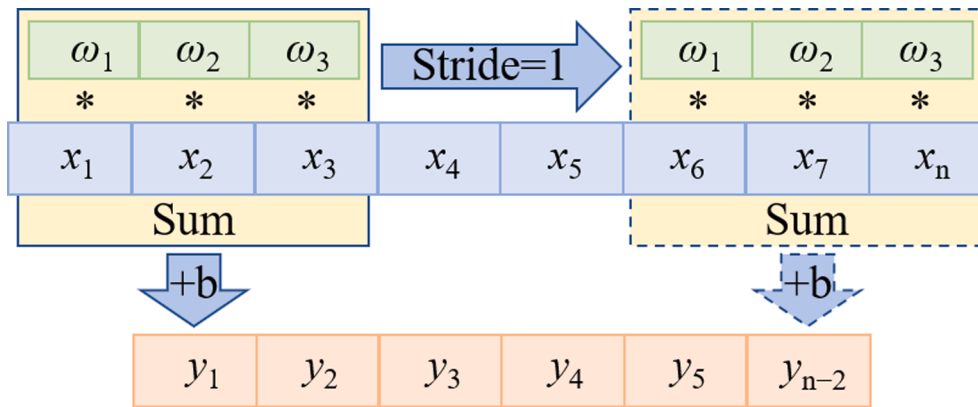


Fig. 1. Illustration of the 1-D convolution operation.

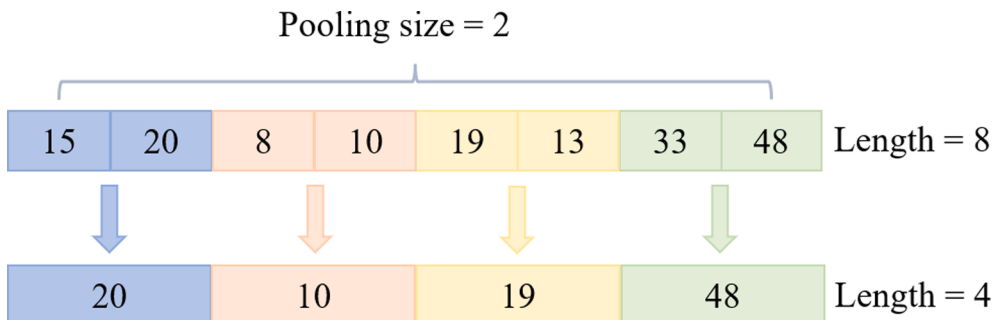


Fig. 2. Illustration of the 1-D max-pooling operation.

model for stress identification of steel components. The designed 1-D CNNs are mainly comprised of the convolutional layers, pooling layers, activation layers, and fully connected layers whose functions are introduced below.

2.1.1. Convolutional layer

The convolutional layer is used to extract features from input signals. There are multiple convolutional kernels in a 1-D convolutional layer, and different convolutional kernels extract different features of the input signal. Weight sharing is used in the 1-D convolutional layer, which can reduce the number of network parameters and make the network converge faster. The 1-D convolutional layer is computed with Eq. (1):

$$x_j^l = f \left(\sum_{i=1}^N x_i^{l-1} \cdot k_{ij}^l + b_j^l \right) \quad (1)$$

where x_j^l is the j th feature map of the l th layer, N denotes the number of input feature maps, $f(\cdot)$ denotes the activation function, \bullet denotes the convolution operation, k_{ij}^l denotes the element of a trainable convolution kernel, and b_j^l denotes the j th threshold of the l th layer.

Fig. 1 shows an example of the one-dimensional convolution operation with a convolution kernel size of 3×1 . The input signal is multiplied by the weights in the convolution window, and the product is summed and a threshold b is added to obtain the output value. In the example, the characteristic value, y_4 , is calculated in the following way: $y_4 = (\omega_1 x_4 + \omega_2 x_5 + \omega_3 x_6)$.

2.1.2. Pooling layer

Pooling layer can shorten the length of the input signal, accentuate the signal features and enhance computation efficiency. Pooling layer can also improve spatial invariance to some degree, including the scale invariance, deformation invariance, and translation invariance [27]. The pooling layer includes two operations: the max-pooling and average

pooling. The max-pooling outputs the largest parameter in the default window and the average pooling outputs the mean of the parameters in the default window.

The pooling layer can also solve the overfitting problem of networks as well. Fig. 2 shows the operation of the 1-D max-pooling with an input feature map size of 8×1 , a pooling window size of 2×1 , and a step length of 2. The largest value in each window is selected as the output and the size of the output feature map is 4×1 .

2.1.3. Activation function

The ReLU activation function is adopted in the study to accelerate convergence and avoid overfitting, as shown in Eq. (2):

$$f(x) = \max(0, x) \quad (2)$$

2.1.4. Fully connected layer

The fully connected layer is a vital component of the 1-D CNN. It is usually implemented at the end of the network along with a softmax or linear regression function to output the prediction results. Each node in the fully connected layer is connected to all nodes of its previous layer, which implies that each node receives all information from the previous convolutional and pooling layers. This means that the final prediction is based on the entire input signal, not just the output of some convolutional or pooling layers [28].

2.2. Loss function

The loss function is used to calculate the difference between the true value and the predicted value of the network and it is crucial to select a suitable loss function for the model to converge fast. Two commonly used loss functions, including the mean square error (MSE) and mean absolute error (MAE), are compared in the study, and the formula is shown in Eq. (3) and Eq. (4), respectively.

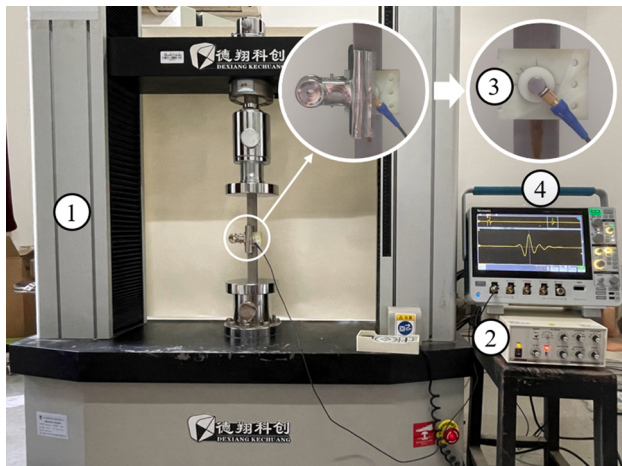


Fig. 3. Stress measurement system.

$$MSE = \frac{1}{n} \sum_{i=1}^n (y_p^i - y_a^i)^2 \quad (3)$$

$$MAE = \frac{1}{n} \sum_{i=1}^n |y_p^i - y_a^i| \quad (4)$$

where y_p^i is the predicted stress, y_a^i is the actual stress, and n is the number of ultrasonic samples.

2.3. Optimizer

The common optimization algorithms used for training the CNN models include the RMSProp and Adam. The RMSProp was proposed mainly to solve the problem of decreasing learning rate in the AdaGrad algorithm [29], and the gradient update rule of the RMSProp algorithm is as follows:

$$s_t = \gamma s_{t-1} + (1 - \gamma) g_t^2 \quad (5)$$

$$x_t = x_{t-1} - \frac{\eta}{\sqrt{s_t + \epsilon}} \odot g_t \quad (6)$$

where η is the learning rate, usually adopting a value of 0.001, and ϵ is a constant (e.g., 10^{-6}) used to maintain numerical stability, γ is defaulted

to be 0.9, s_t is the state variable of the RMSProp algorithm, and g_t is the gradient of the RMSProp algorithm.

The Adam algorithm [30], which is simple to implement and requires very little memory, makes use of the advantages of the AdaGrad algorithm to handle sparse gradients and the RMSProp algorithm to handle non-smooth targets. Unlike the RMSProp algorithm, the Adam algorithm uses a bias correction method to make the gradient converge to the correct direction at a very fast rate. The update process can be simply expressed as follows:

$$m_{t+1} = \alpha m_t + (1 - \alpha) \Delta x_t \quad (7)$$

$$v_{t+1} = \beta v_{t+1} + (1 - \beta) (\Delta x_t)^2 \quad (8)$$

$$\Delta x_{t+1} = - lr \frac{m_{t+1}}{\sqrt{v_{t+1}} + \epsilon} \quad (9)$$

where $\alpha = 0.9$ and $\beta = 0.999$ are the default exponential decay rates for the first-order moment and second-order moment estimation. $\epsilon = 10^{-8}$ is the default value used to maintain numerical stability during the optimization process. lr represents the learning rate during the training process. In the study, these two optimization algorithms are applied to train the 1-D CNN separately and their performances are compared.

3. Experimental studies

In the part, the equipment and steel components used in the experiment are described first, and followed is the introduction on the details of experiments, and finally, the procedures for stress identification of steel components and the corresponding results are introduced.

3.1. Equipment and steel components

To accurately collect the ultrasonic signals of steel components under different stress levels, a loading and measurement system was designed in the present study. Fig. 3 and Fig. 4 show the overall diagram and equipment connection diagram of the loading and measurement system, respectively. As can be seen from Fig. 3, the system consists of four parts, including the universal testing machine (DWD-2000, Sichuan Dexiang Kechuang Instrument Co., Ltd.), the ultrasonic generator (JSR DDR300), the shear-wave transceiver probe (Olympus V156, center frequency: 5 MHz), and the oscilloscope (Tektronix MDO34, bandwidth: 200 MHz, sampling rate: 2.5 GS/s). In addition, the probe was coupled to the

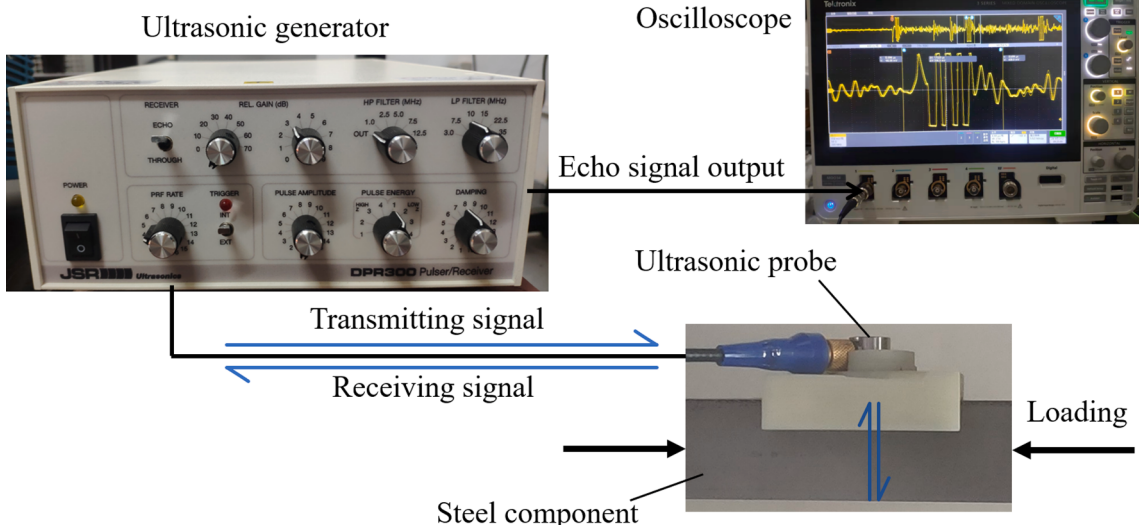


Fig. 4. Connection of instruments.

Table 2
Size and amount of steel components.

Steel component	Size (mm)	Amount
B	240 × 25 × 16	1
C	240 × 25 × 18	1
D	240 × 25 × 20	1
E	240 × 25 × 22	1
F	240 × 25 × 24	1

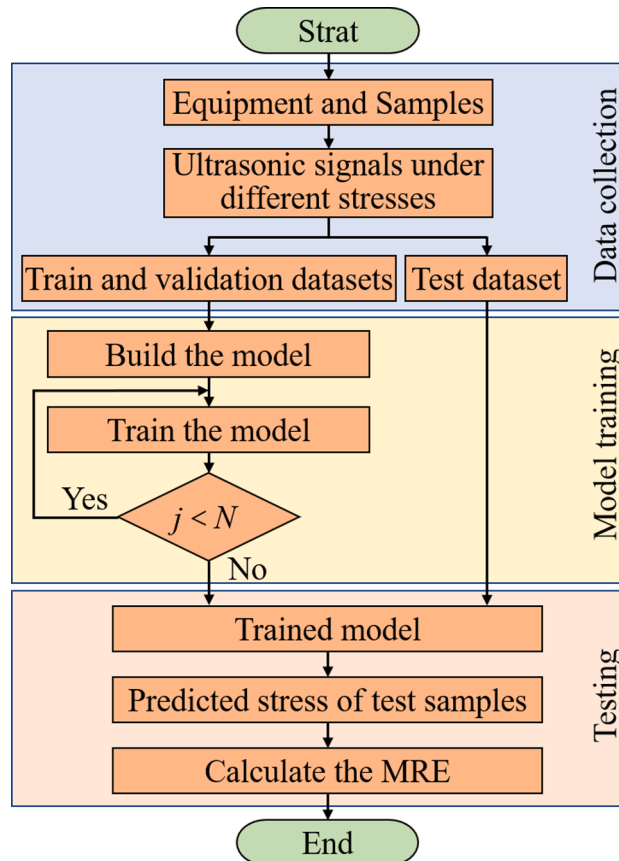


Fig. 5. Flowchart of the proposed methodology for stress identification.

surface of the steel component through the Olympus SWC-2 2 oz type ultrasound coupler to ensure a good connection between them and reduce the wear of the probe as it moves.

Fig. 4 shows the process of collecting ultrasonic signals from steel components under different stresses. The ultrasonic generator emits pulse signals shunting into the transceiver probe to generate a pure transverse wave. The pure transverse wave propagates along the thickness direction of the steel component and is then reflected from the back of the component. The echo signal is collected by the same probe and transmitted to the ultrasonic generator and displayed on the oscilloscope.

The steel components were made of 45# steel with a yield strength of 345 MPa. Five steel components with different sizes were used in the experiment, as shown in Table 2. The experiment was carried out at room temperature (14 °C) and the variation of temperature was not considered during the experiment.

3.2. Implementation details

3.2.1. Computation configuration and evaluation index

The experiment was conducted with a computer (Central Processing Unit (CPU): Intel i5-9600 k @3.20 GHz, Graphics Processing Unit (GPU):

NVIDIA GeForce RTX 3060 with 12 GB memory) under the GPU mode based on the TensorFlow framework. The software configuration is the Windows 10 system installed with Python 3.7.4, Tensorflow-gpu 2.4.1 and Keras 2.4.3. The initial parameters of each layer of the 1-D CNN were randomly initialized by the Glorot uniform distribution [31].

The relative error (RE) is defined in Eq. (10). The mean relative error (MRE) is the average of the REs, as shown in Eq. (11).

$$RE = \frac{|y_p - y_a|}{y_a} \times 100\% \quad (10)$$

$$MRE = \frac{\sum_{i=1}^n RE_i}{n} \quad (11)$$

where y_p is the predicted stress of each test sample, y_a is the actual stress of each test sample, RE_i is the relative error of the i th test sample, and n is the number of test samples.

The stress identification process for steel components is shown in Fig. 5, where j denotes the number of current training epoch and N denotes the overall number of preset epochs.

3.2.2. Determination of shear-wave polarization angle

As shown in Fig. 6(a), the ultrasonic shear-wave probe is fixed on the steel component, and the contact point of the probe and the steel component is adopted as the origin to establish the Cartesian coordinate system, in which the polarization angle is the angle between the polarization direction of the ultrasonic shear wave and the x -axis, and the propagation direction of the ultrasonic shear wave is the y -axial direction.

Euclidean distance is often used to measure the similarity between signals [32], which is also adopted in the present study to measure the similarity between two ultrasonic signals obtained under different stress levels. Assuming that $p_1 = (x_{11}, x_{12}, x_{13}, \dots, x_{1n})$ and $p_2 = (x_{21}, x_{22}, x_{23}, \dots, x_{2n})$ are two ultrasonic signals obtained under different stress levels in the time domain, the Euclidean distance d between the two signals can be calculated with Eq. (12).

$$d = \sqrt{\sum_{i=1}^n (x_{1i} - x_{2i})^2} \quad (12)$$

Usually, a larger Euclidean distance between two ultrasonic signals indicates a bigger difference between them and vice versa. Therefore, an optimal shear-wave polarization angle can be determined under the condition that the Euclidean distances between ultrasonic signals obtained under different stress levels achieve bigger values.

In the present study, the procedures to determine the optimal shear-wave polarization angle are summarized as follows. Firstly, the ultrasonic shear-wave probe was fixed on the surface of a steel component with the polarization angle of 0° and five ultrasonic signals were collected at each of the eight stress levels ranging from 0 to 140 MPa with an interval of 20 MPa. Fig. 7 illustrates one of the collected ultrasonic signals. Then, one ultrasonic sample was obtained by averaging the five ultrasonic signals collected at each stress level and the Euclidean distance between every two of the eight samples was calculated. A total of 28 Euclidean distances were obtained at the polarization angle of 0°, as listed in Table 3, in which 3.74 MPa represents the Euclidean distance between the two ultrasonic samples obtained at the stress level of 0 and 20 MPa, respectively. The total Euclidean distance corresponding to the polarization angle of 0° was obtained by summing these 28 Euclidean distances. Finally, the polarization angle was adjusted from 0° to 90° with an interval of 15° and at each polarization angle, the above two steps were conducted to obtain the total Euclidean distance corresponding to each of the polarization angles under consideration, as shown in Table 4. It can be observed from Table 3 that the total Euclidean distance achieves the largest value at the polarization angle of 45°, indicating that the difference between the ultrasonic signals obtained under different stress levels is the most distinguishable at the

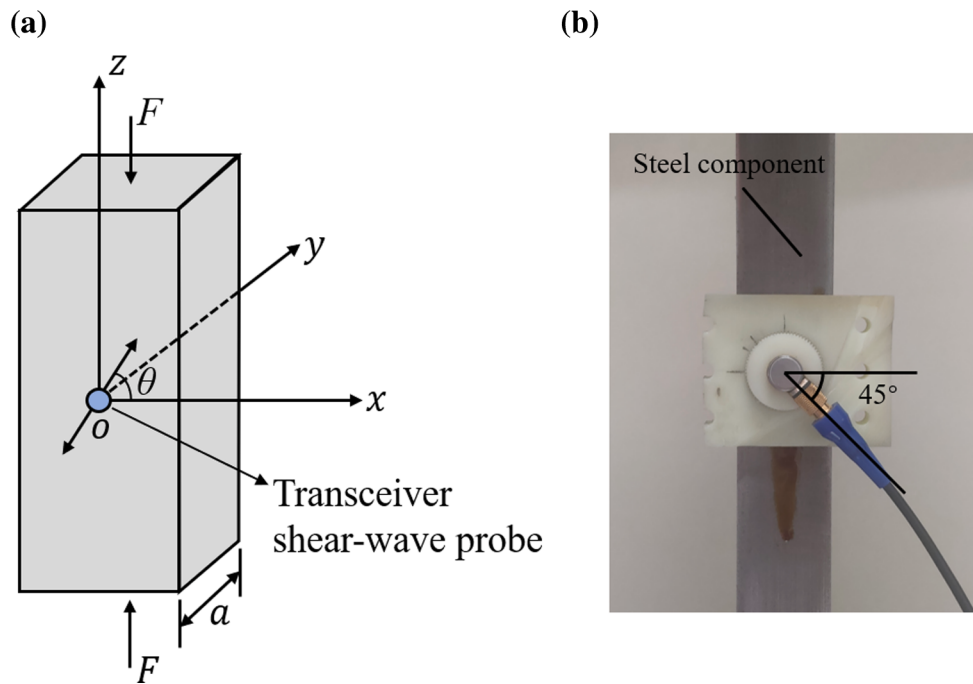


Fig. 6. Illustration of ultrasonic shear-wave polarization angle (θ), (a) Cartesian coordinate system schematic diagram, (b) shear-wave polarization angle.

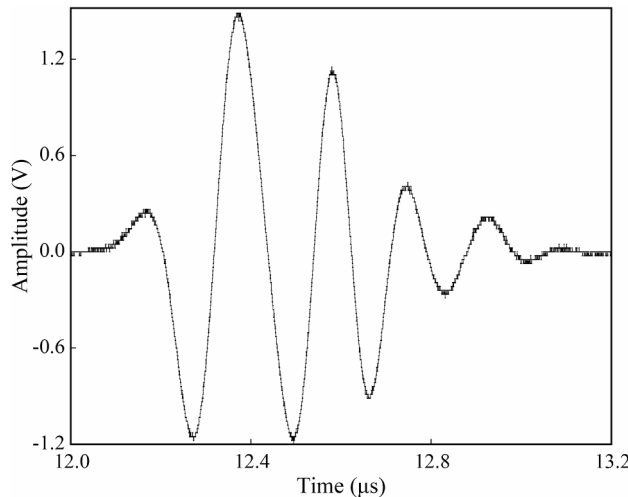


Fig. 7. Illustration of the collected ultrasonic signal.

Table 3
Twenty-eight Euclidean distances at the polarization angle of 0° (unit: MPa).

Stress (MPa)	20	40	60	80	100	120	140
0	3.74	4.15	8.28	8.83	9.67	10.62	11.76
20		0.98	4.86	5.46	6.34	7.34	8.58
40			4.52	5.07	5.90	6.89	8.15
60				0.91	1.69	2.70	4.04
80					1.14	2.15	3.59
100						1.10	2.60
120							1.70



Fig. 8. Illustration of five steel components under consideration.

Table 4
Total Euclidean distances obtained under seven considered polarization angles.

Polarization angle ($^\circ$)	0	15	30	45	60	75	90
Total Euclidean distance (MPa)	142.75	123.90	177.44	613.86	511.93	367.39	253.53

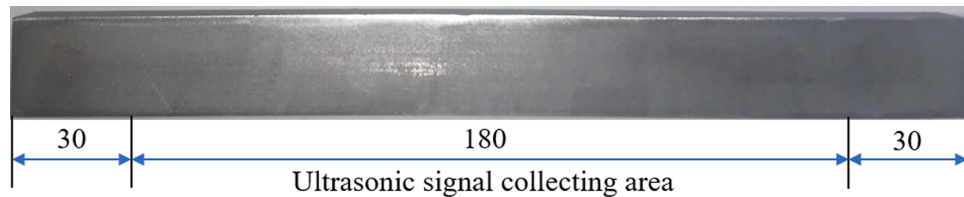


Fig. 9. Illustration of the area for ultrasonic signal collection (unit: mm).

polarization angle of 45° . Therefore, the shear-wave polarization angle was taken as 45° in the present study, as shown in Fig. 6(b).

3.3. Stress identification of steel components

3.3.1. Dataset preparation

To identify the stress of steel components based on the deep learning algorithm, an ultrasonic signal dataset needs to be prepared in advance. The preparation of the ultrasonic signal dataset includes three steps.

The first step is the preparation of steel components. Five steel components with different thicknesses were fabricated and denoted with B, C, D, E and F in order, as shown in Fig. 8. The surfaces of the five specimens were polished to guarantee a good connection between the probe and steel components. Three different points on the surface of each steel component were selected to collect the ultrasonic signals to build the training, validation and test datasets.

In the second step, the training and validation datasets were established. A universal testing machine with a loading range of 200 kN was used to conduct uniaxial compression tests in the laboratory, as shown in Fig. 3. Ten compressive stresses ranging from 0 to 300 MPa (0, 10, 20, 40, 60, 80, 120, 160, 220 and 300 MPa) were applied to the prepared steel components and the ultrasonic signals of the steel components under each stress level were collected after the loading was stable. Under each stress level, 20 ultrasonic signals were collected at each point and each signal has a size of 3000×1 with a sampling frequency of 2.5 GS/s, as shown in Fig. 7. Considering the uneven stress at the two ends of the steel component, all ultrasonic signals were collected within the area far away from the two ends of the steel component, as shown in Fig. 9. A total of 3000 ultrasonic samples ($20 \times 3 \times 5 \times 10$) were collected from all the considered steel components under ten stress levels, which were then divided into the training and validation datasets according to the ratio of 4:1. Therefore, the number of ultrasonic samples in the training and validation datasets were 2400 and 600, respectively. It should be noted that the yield strength of 45# steel is 345 MPa, which means that the steel components will not yield during the uniaxial compression test. It should also be noted that according to Euler's formula, the critical buckling stress of the steel component was calculated to be 1,142 MPa, which indicates that the steel component will not buckle during the uniaxial compression test.

The third step is the establishment of the test dataset, which would be used to evaluate the performance of the trained 1-D CNN. Nine different stresses (including 14, 30, 52, 74, 96, 142, 196, 260 and 306 MPa) were applied to the steel components through the uniaxial compression test and the corresponding ultrasonic signals were collected to establish the test dataset, in which each test sample was obtained by averaging ten ultrasonic signals to improve the signal-to-noise ratio [33]. Under each stress level, 20 ultrasonic signals were collected at each position of the five steel components under consideration. Thus, a total of 270 ultrasonic samples ($20/10 \times 3 \times 5 \times 9$) were obtained for the test dataset.

3.3.2. Determination of the optimal 1-D CNN architecture for stress identification of steel components

The three designed networks were trained, validated, and tested, respectively, using the ultrasonic datasets of steel components obtained in the previous section with the same hyperparameters (loss function:

Table 5

The MRE and training time of the three designed 1-D CNNs for stress identification of steel components.

Designed 1-D CNNs	MRE (%)	Training time (s/epoch)
Shadow	8.11	1.25
Medium	6.96	1.73
Deep	12.74	2.59

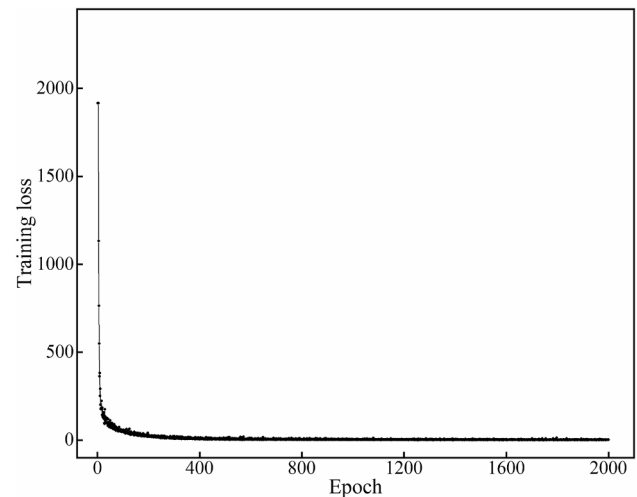


Fig. 10. Variation of training loss against the number of epochs under initial parameters.

MSE, optimizer: Adam, batch size = 8, epoch = 2000). The AE and training time of the three networks for stress identification of steel components are compared and the comparison results are shown in Table 5. It can be seen from Table 5 that the medium 1-D CNN can make a better balance between the stress identification accuracy and the computation efficiency and was thus adopted for the following analysis.

3.3.3. Parameter optimization

The loss function, optimizer and batch size of the network have a significant influence on the performance of the 1-D CNN [34]. In the present study, two loss functions (MSE and MAE), two optimizers (Adam and RMSProp), and six batch sizes (8, 16, 32, 64, 128, and 256) were considered and the performance of the medium 1-D CNN was investigated under the 24 combinations of the three hyperparameters. With the loss function of MSE, optimizer of Adam and batch size of 8, the variation of training loss against the number of epochs is shown in Fig. 10, which shows that the training loss decreases sharply at first and gradually stabilizes when the epoch reaches around 1,200. Therefore, the number of epochs was taken as 1,200.

The performance of the 1-D CNN under the 24 cases considered is shown in Fig. 11 and Table 6, from which it can be seen that the loss function, optimizer, and batch size have a coupling effect on the MREs. The minimum MREs for stresses of 14, 30, 52, 74, 96, 142, 196, 260 and 306 MPa are 8.50% for Case 4, 5.79% for Case 4, 4.45% for Case 4,

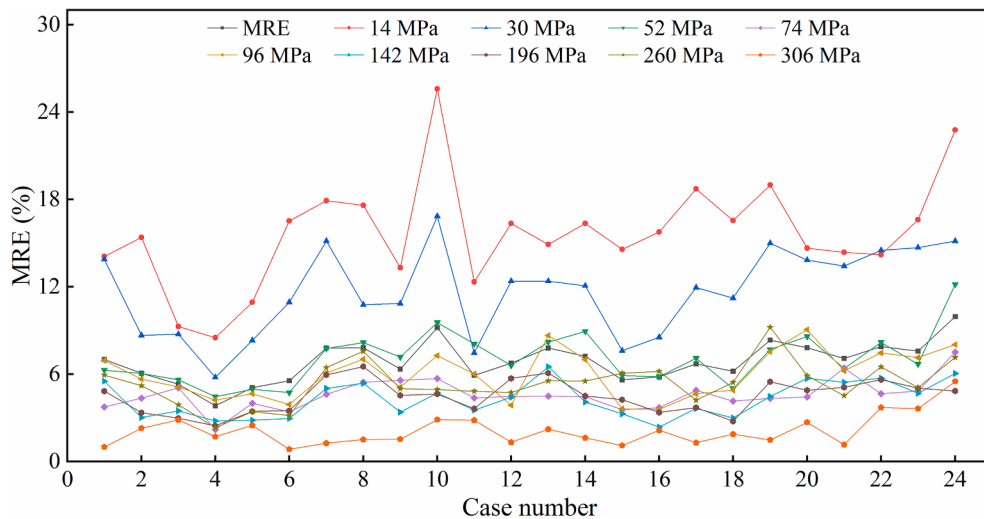


Fig. 11. MREs of test dataset under 24 cases.

Table 6

Parameters considered and corresponding MREs for each stress level in the test dataset.

Cases	Loss function	Optimizer	Batch size	MREs (%) for different stresses (MPa)								MRE (%)	
				14	30	52	74	96	142	196	260		
1	MSE	Adam	8	14.09	13.88	6.28	3.75	6.94	5.52	4.84	5.94	1.00	7.00
2			16	15.40	8.67	6.05	4.36	5.66	3.02	3.36	5.21	2.29	6.07
3			32	9.28	8.74	5.62	5.07	5.13	3.48	2.98	3.90	2.86	5.32
4			64	8.50	5.79	4.45	2.21	4.23	2.80	2.46	2.32	1.71	3.83
5			128	10.94	8.31	4.97	4.01	4.67	2.84	3.45	3.43	2.48	5.09
6			256	16.52	10.94	4.74	3.42	3.91	2.96	3.49	3.16	0.85	5.56
7		RMSProp	8	17.91	15.15	7.76	4.62	6.08	5.02	5.96	6.45	1.26	7.80
8			16	17.59	10.77	8.18	5.45	7.02	5.38	6.53	7.58	1.52	7.82
9			32	13.31	10.86	7.17	5.58	5.11	3.39	4.54	5.00	1.54	6.35
10			64	25.60	16.85	9.55	5.71	7.28	4.71	4.65	4.95	2.89	9.20
11	MAE	Adam	128	12.33	7.46	8.08	4.37	6.01	3.54	3.64	4.83	2.84	5.92
12			256	16.35	12.39	6.60	4.47	3.88	4.42	5.71	4.74	1.32	6.75
13			8	14.91	12.39	8.21	4.49	8.66	6.51	6.08	5.54	2.22	7.79
14			16	16.35	12.07	8.94	4.45	7.01	4.09	4.51	5.53	1.63	7.23
15			32	14.58	7.61	5.91	3.56	3.61	3.28	4.25	6.07	1.10	5.61
16			64	15.76	8.53	5.84	3.70	3.59	2.37	3.38	6.19	2.15	5.82
17			128	18.73	11.95	7.10	4.89	4.65	3.65	3.71	4.22	1.29	6.71
18			256	16.56	11.23	5.01	4.15	4.90	3.00	2.78	5.43	1.88	6.20
19		RMSProp	8	18.99	15.00	7.69	4.33	7.55	4.48	5.48	9.23	1.49	8.34
20			16	14.65	13.84	8.59	4.44	9.07	5.71	4.89	5.90	2.70	7.82
21			32	14.37	13.43	6.39	6.42	6.23	5.46	5.10	4.52	1.16	7.08
22			64	14.21	14.51	8.19	4.65	7.46	5.74	5.63	6.50	3.72	7.90
23			128	16.60	14.69	6.69	4.84	7.14	4.69	5.04	5.08	3.63	7.59
24			256	22.77	15.14	12.16	7.51	8.04	6.05	4.85	7.16	5.50	9.96

2.21% for Case 4, 3.59% for Case 16, 2.37% for Case 16, 2.46% for Case 4, 2.32% for Case 4 and 0.85% for Case 6, respectively. Case 4 was chosen as the optimal model which achieved the lowest MRE of 3.83% for all the test samples under consideration. The loss function, optimizer and batch size in Case 4 are MSE, Adam and 64, respectively. It should be noted that the traditional ultrasonic shear wave-based methods can only detect the absolute stress of steel components with a single thickness with a MRE of 5% or less. If these methods were used to detect the absolute stress of steel components with another different thickness, the theoretical formula needs to be recalibrated using components with the same thickness and the new formula can only be used to identify the stress of components with this same thickness. However, the proposed method can handle steel components with different thicknesses while it only needs to train the model once. This indicates that the proposed method has better applicability than the traditional ultrasonic shear wave-based method while achieving the same level of accuracy under the same circumstances.

The predicted and actual stresses of the test samples in Case 4 are

shown in Fig. 12 and the MREs of test samples under each stress level are shown in Fig. 13, which shows that the MRE generally decreases from 8.50% to 1.71% as the stress increases from 14 to 306 MPa. It can be observed from Fig. 13 and Table 6 that the predicted MRE of the model for identification of 14 MPa in the test samples is significantly higher than that of other stresses in the test samples, which is due to the fact that the stress value of 14 MPa is relatively small and tends to result in a large relative error in the calculation even if the absolute error of the predicted stress is small. It can also be observed from Fig. 12 that the predicted stress of most test samples of 306 MPa is lower than their actual stress, as they are beyond the stress range of the training samples (from 0 to 300 MPa). The results show that the proposed method has good robustness for stress identification of steel components and that a smaller MRE can be obtained when the steel components experience larger stress.

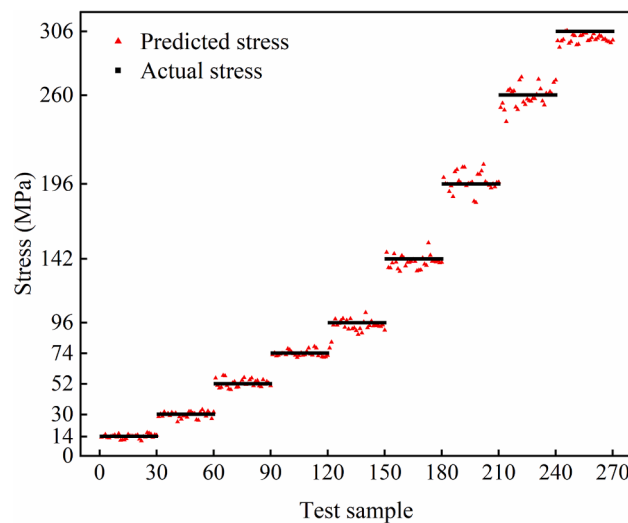


Fig. 12. Predicted stress and actual stress of test samples.

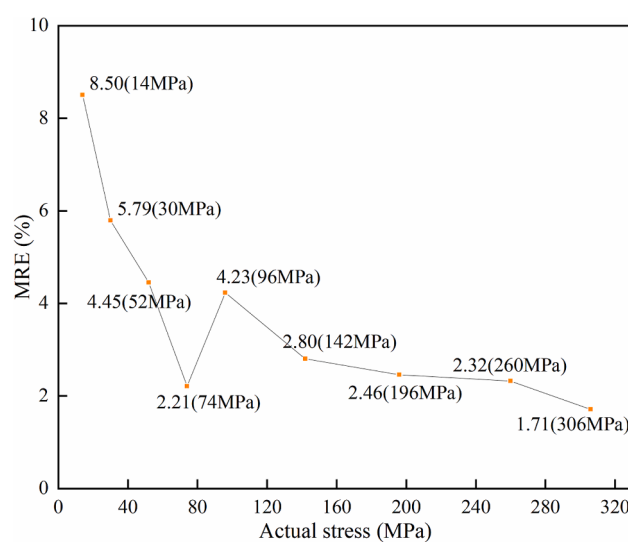


Fig. 13. MREs of test samples under each stress level considered.

4. Conclusions

A new approach is proposed for stress identification of steel components with different thicknesses based on the deep learning and ultrasonic method in the present study. Firstly, uniaxial compression tests were conducted on five steel components with different thicknesses. Three thousand ultrasonic signals of steel components were collected under ten compressive stresses (0, 10, 20, 40, 60, 80, 120, 160, 220 and 300 MPa) and used to prepare the training and validation datasets. Two hundred and seventy ultrasonic samples of steel components were obtained under nine different compressive stresses (14, 30, 52, 74, 96, 142, 196, 260 and 306 MPa) and used to prepare the test dataset. Secondly, three 1-D CNN models with different architectures were designed, trained and tested with the prepared datasets and the optimal architecture for stress identification of steel components was determined. Finally, the parameters of the 1-D CNN model with the optimal architecture were then optimized and verified with the test dataset. The results showed that the 1-D CNN-based deep learning model can be used to establish the relationship between the characteristics of ultrasonic signals and the absolute stresses experienced by steel components with different thicknesses. The following conclusions can be drawn from the

study:

1. The 1-D CNN with six convolutional layers is the optimal model that can achieve a satisfactory balance between the stress identification accuracy and computational efficiency.
2. The proposed optimal 1-D CNN model can accurately predict the absolute stress of steel components with different thicknesses, and the mean relative error is 3.83% for all the test samples under consideration, which provides a good reference for stress detection of steel structures.
3. For absolute stress identification of steel components, the proposed optimal 1-D CNN model tends to achieve lower relative error as the steel components experience larger stress.

In practical engineering, structural steel components often work in complex environmental conditions and the influences of temperature, coupling medium, surface condition of components on the detection accuracy should also be investigated in the future.

CRediT authorship contribution statement

Lu Deng: Conceptualization, Methodology. **Shaopeng Xu:** . Wei Wang: Writing – original draft, Writing – review & editing. **Chao Xiang:** Software, Validation.

Declaration of Competing Interest

The authors declare that they have no known competing financial interests or personal relationships that could have appeared to influence the work reported in this paper.

References

- [1] J. Li, H. Hao, K. Fan, J. Brownjohn, Development and application of a relative displacement sensor for structural health monitoring of composite bridges, *Struct. Control Health Monit.* 22 (4) (2015) 726–742, <https://doi.org/10.1002/stc.1714>.
- [2] L.E. Aygun, V. Kumar, C. Weaver, M. Gerber, S. Wagner, N. Verma, B. Glisic, J. C. Sturm, Large-area resistive strain sensing sheet for structural health monitoring, *Sensors* 20 (5) (2020) 1386, <https://doi.org/10.3390/s20051386>.
- [3] V. Lamour, A. Haouas, J. Dubois, et al., Long term monitoring of large massive concrete structures cumulative effects of thermal gradients, *Non-Destructive Testing in Civil Engineering*, Nantes, France, 2009.
- [4] G. Ruibin, D. Wenjian, Q. Fei, Y.u. Min, Z. Weigang, Welding residual stress measurement of an urban buried gas pipeline by X-ray diffraction method, *Insight (Northampton)* 57 (10) (2015) 556–561, <https://doi.org/10.1784/insi.2015.57.10.556>.
- [5] L. Mierczak, D.C. Jiles, G. Fantoni, A new method for evaluation of mechanical stress using the reciprocal amplitude of magnetic Barkhausen noise, *IEEE Trans. Magn.* 47 (2) (2011) 459–465, <https://doi.org/10.1109/TMAG.2010.2091418>.
- [6] M. Roskosz, Metal magnetic memory testing of welded joints of ferritic and austenitic steels, *NDT and E Int.* 44 (3) (2011) 305–310, <https://doi.org/10.1016/j.ndteint.2011.01.008>.
- [7] W. Song, C. Xu, Q. Pan, J. Song, Nondestructive testing and characterization of residual stress field using an ultrasonic method, *Chin. J. Mech. Eng.* 29 (2) (2016) 365–371, <https://doi.org/10.3901/CJME.2015.1023.126>.
- [8] D.S. Hughes, J.L. Kelly, Second-order elastic deformation of solids, *Phys. Rev.* 92 (5) (1953) 1145–1149.
- [9] R.W. Benson, V.J. Raelson, Acoustoelasticity, *Prod. Eng. Res. Devel.* 30 (1959) 56–59.
- [10] N.N. Hsu, Acoustical birefringence and the use of ultrasonic waves for experimental stress analysis, *Exp. Mech.* 14 (5) (1974) 169–176.
- [11] J.-Y. Chatellier, M. Touratier, A new method for determining acoustoelastic constants and plane stresses in textured thin plates, *J. Acoust. Soc. Am.* 83 (1) (1988) 109–117.
- [12] M. Hasegawa, Y. Sasaki, Acoustoelastic birefringence effect in wood I: effect of applied stresses on the velocities of ultrasonic shear waves propagating transversely to the stress direction, *J. Wood Sci.* 50 (1) (2004) 47–52, <https://doi.org/10.1007/s10086-003-0536-8>.
- [13] Z. Li, J. He, J. Teng, Y. Wang, Internal stress monitoring of in-service structural steel members with ultrasonic method, *Materials* 9 (4) (2016) 223, <https://doi.org/10.3390/ma9040223>.
- [14] Z. Li, J. He, J. Teng, Q. Huang, Y. Wang, Absolute stress measurement of structural steel members with ultrasonic shear-wave spectral analysis method, *Struct. Health Monit.* 18 (1) (2019) 216–231, <https://doi.org/10.1177/1475921717746952>.

- [15] J. He, Z. Li, J. Teng, M. Li, Y. Wang, Absolute stress field measurement in structural steel members using the Lcr wave method, *Measurement* 122 (2018) 679–687, <https://doi.org/10.1016/j.measurement.2018.03.022>.
- [16] J. He, Z. Li, J. Teng, et al., Comparison of the Lcr wave TOF and shear-wave spectrum methods for the uniaxial absolute stress evaluation of steel members, *Struct. Control Health Monit.* 26 (2019), e2348, <https://doi.org/10.1002/stc.2348>.
- [17] X. Zhang, K. Wang, Y. Wang, et al., An improved method of rail health monitoring based on CNN and multiple acoustic emission events, in: 2017, pp.1-6. IEEE. DOI: 10.1109/I2MTC.2017.7969693.
- [18] D. Li, Y. Wang, W.-J. Yan, W.-X. Ren, Acoustic emission wave classification for rail crack monitoring based on synchrosqueezed wavelet transform and multi-branch convolutional neural network, *Struct. Health Monit.* 20 (4) (2021) 1563–1582, <https://doi.org/10.1177/1475921720922797>.
- [19] Z. Chen, C. Li, R. Sanchez, Gearbox fault identification and classification with convolutional neural networks, *Shock Vib.* 2015 (2015) 1–10, <https://doi.org/10.1155/2015/390134>.
- [20] S. Kim, J.-H. Choi, Convolutional neural network for gear fault diagnosis based on signal segmentation approach, *Struct. Health Monit.* 18 (5-6) (2019) 1401–1415, <https://doi.org/10.1177/1475921718805683>.
- [21] W. Wang, P. Shi, H. Chu, L.u. Deng, B. Yan, Deep learning framework for total stress detection of steel components, *J. Bridge Eng.* 26 (1) (2021) 04020113, [https://doi.org/10.1061/\(ASCE\)BE.1943-5592.0001655](https://doi.org/10.1061/(ASCE)BE.1943-5592.0001655).
- [22] H. Wu, J. Chen, X. Liu, Y. Xiao, M. Wang, Y.i. Zheng, Y. Rao, One-dimensional CNN-based intelligent recognition of vibrations in pipeline monitoring with DAS, *J. Lightwave Technol.* 37 (17) (2019) 4359–4366, <https://doi.org/10.1109/JLT.2019.2923839>.
- [23] Y. Zhang, Y. Miyamori, S. Mikami, T. Saito, Vibration-based structural state identification by a 1-dimensional convolutional neural network, *Comput.-Aided Civ. Infrastruct. Eng.* 34 (9) (2019) 822–839.
- [24] L. Eren, Bearing fault detection by one-dimensional convolutional neural networks, *Math. Problems Eng.* 2017 (2017) 1–9, <https://doi.org/10.1155/2017/8617315>.
- [25] Y.-J. Cha, W. Choi, O. Büyüköztürk, Deep learning-based crack damage detection using convolutional neural networks, *Comput.-Aided Civ. Infrastruct. Eng.* 32 (5) (2017) 361–378.
- [26] M.G. Ragab, S.J. Abdulkadir, N. Aziz, Q. Al-Tashi, Y. Alyousifi, H. Alhussain, A. Alqushaibi, A novel one-dimensional CNN with exponential adaptive gradients for air pollution index prediction, *Sustainability* 12 (23) (2020) 10090, <https://doi.org/10.3390/su122310090>.
- [27] X. Zhao, J.S. Casals, B. Li, et al., Classification of epileptic iEEG signals by CNN and data augmentation, in: IEEE International Conference on Acoustics, Speech and Signal Processing (ICASSP) 2020, pp.926-930.
- [28] J. Gu, Z. Wang, J. Kuen, L. Ma, A. Shahroudy, B. Shuai, T. Liu, X. Wang, G. Wang, J. Cai, T. Chen, Recent advances in convolutional neural networks, *Pattern Recogn.* 77 (2018) 354–377.
- [29] T. Tieleman, G. Hinton, Lecture 6.5-rmsprop: Divide the gradient by a running average of its recent magnitude, 2012, pp. 26-31.
- [30] P. KD, J. B, Adam: a method for stochastic optimization, 2014, arXiv:1412.6980.
- [31] X. Glorot, Y. Bengio, Understanding the difficulty of training deep feedforward neural networks, in: Proceedings of the thirteenth international conference on artificial intelligence and statistics 2010, pp. 249-256.
- [32] J. Yu, J. Amores, N. Sebe, et al., A new study on distance metrics as similarity measurement, in: IEEE International Conference on Multimedia and Expo. 2006, pp.533-536.
- [33] H.J. Lim, H. Sohn, Online stress monitoring technique based on Lamb-wave measurements and a convolutional neural network under static and dynamic loadings, *Exp. Mech.* 60 (2) (2020) 171–179, <https://doi.org/10.1007/s11340-019-00546-8>.
- [34] E. Karaaslan, U. Bagci, F.N. Catbas, Attention-guided analysis of infrastructure damage with semi-supervised deep learning, *Autom. Constr.* 125 (2021) 103634, <https://doi.org/10.1016/j.autcon.2021.103634>.